STUDIA UBB CHEMIA, LXIX, 2, 2024 (p. 7-17)
(RECOMMENDED CITATION)
DOI:10.24193/subbchem.2024.2.01

COMPARATIVE PHASE EVOLUTION, MORPHOLOGICAL AND OPTICAL ANALYSIS OF PARTIALLY STABILIZED ZIRCONIA CERAMICS

Claudia Andreea COJAN[a], Réka BARABÁS[b], Marieta MUREȘAN-POP[c,d], Liliana BIZO[a,c,*]

ABSTRACT. Partially stabilized zirconia (PSZ) ceramics are one of the most important materials used for different applications like thermal barrier coatings, refractories, oxygen-permeating membranes, and dental and bone implants. In this work, the structural, morphological, and optical properties of bulk Mg-PSZ, Ca-PSZ, and Ce-PSZ, prepared by solid state reaction at high temperature, were comparatively evaluated. Laser diffraction analyses revealed particles by thousands orders of magnitude larger compared to crystallite sizes determined from X-ray powder diffraction (XRPD), more evidenced in the case of Ca-PSZ. The structural analyses indicated the presence of both *m*- and *t*-ZrO_2 phases, in different ratios, depending on the doping cation. The scanning electron microscopy (SEM) micrographs confirmed the homogenous distribution of the elements through mixed oxides. Further, optical properties evaluated in terms of ultraviolet–visible diffuse reflectance spectroscopy (UV-VIS DRS) revealed that the doped ZrO_2 samples showed a smaller bandgap compared with pure ZrO_2, which may be due to the incorporation of magnesia, calcia or ceria in the ZrO_2 matrix. The maximum bandgap reduction of ZrO_2 was observed on Ca-PSZ, having a value of 3.52 eV.

Keywords: *partially stabilized zirconia, solid state reaction, structural properties, optical properties*

[a] *Department of Chemical Engineering, Babeş-Bolyai University, 11 Arany Janos Street, RO-400028, Cluj-Napoca, Romania*
[b] *Department of Chemistry and Chemical Engineering of Hungarian Line of Study, Babeş-Bolyai University, 11 Arany Janos Street, RO-400028, Cluj-Napoca, Romania*
[c] *Interdisciplinary Research Institute on Bio-Nano-Sciences, Babeş-Bolyai University, 42 Treboniu Laurian Street, RO-400271, Cluj-Napoca, Romania*
[d] *INSPIRE Research Platform, Babeş-Bolyai University, 11 Arany Janos Street, RO-400028, Cluj-Napoca, Romania*
** Corresponding author: liliana.bizo@ubbcluj.ro*

INTRODUCTION

Besides many ceramic materials, zirconia (ZrO_2), which is also known as “ceramic steel”, has gained a special interest among researchers due to its multiple applications such as catalysts, sensors, and semiconductor devices, and structural materials, such as coatings on cutting tools ceramics, or implants [1]. The most useful mechanical properties can be achieved when zirconia is in a multiphase form or partially stabilized zirconia (PSZ), obtained by adding small amounts of a metal oxide dopant, such as MgO (magnesia), CaO (calcia), Sc_2O_3 (scandia), Y_2O_3 (yttria) and ceria (CeO_2) [1-3].

PSZ are interesting materials due to their fascinating properties like good flexural strength, high toughness, excellent wear resistance, high thermal shock resistance, good ionic conductivity, and biocompatible, finding applications in thermal barrier coatings, refractories, oxygen-permeating membranes, dental and bone implants [4].

About 10 mol% Mg is the percentage most used in industry to obtain Mg-PSZ (magnesia partially stabilized zirconia) [5]. Mg-PSZ exhibits satisfactory thermal shock resistance, high mechanical properties and a small thermal expansion coefficient. MgO or $MgCO_3$ could be used as a stabilizer, and one of the advantages presented by these compounds is that they can be used in humid, high-temperature environments [6]. Ca-PSZ (calcia partially stabilized zirconia) has shown excellent thermal stability and corrosion resistance in extreme environments. It could be used in immersion nozzle refractories for continuous steel casting involving extremely high temperatures (~1500 °C) and corrosive molten flow environments [7-10]. The accessibility of calcium precursors is another aspect that makes the Ca-PSZ an interesting material. CeO_2 nanoparticles have important attention due to their unique characteristics and distinctive properties such as high refractive index, high thermal stability, high hardness, high surface area, UV absorbing ability, facile electrical conductivity, specific chemical reactivity, or large oxygen storage capacity [11]. Stabilizing ZrO_2 with CeO_2 improves the physicochemical properties of zirconia, Ce-PSZ (ceria partially stabilized zirconia) being recognized as a high-toughness ceramic.

The role of Ca and Mg dopant cations in phase stabilization of ZrO_2 has been intensively studied, with Mg emerging as a crucial dopant ion because of its ability to enhance the photocatalytic properties of ZrO_2 [12]. On the other hand, the Ce inclusion in ZrO_2 is expected to reduce thermal conductivity, which would widen the utilization of Ce doped ZrO_2 in thermal barrier coating applications [13]. Even if the phase stability was intensively studied in the last years, the role of alkaline earth and rare earth doping cations in zirconia have been widely examined at present. Thus, a *comparative study* of structural

and optical properties of bulk PSZ, which could provide an insight on the phase stabilization and structure modifications due to the Ca, Mg and Ce-doping in ZrO_2, which has not yet been reported to the best of our knowledge, is necessary.

The present work reported the facile synthesis of bulk Mg-PSZ, Ca-PSZ and Ce-PSZ by solid-state reaction at high temperature. The effect of doping with 10 at% Mg, Ca or Ce on zirconia's structural, morphological and optical properties, determined by different techniques, was comparatively analyzed and discussed.

RESULTS AND DISCUSSION

The particle size distribution (PSD) of the prepared PSZ ceramic powders was analyzed by laser diffraction with the results given in **Figure 1**. From the PSD data presented graphically in the figure there are two types of curves: differential and cumulative. It can be observed that the PSD curves of Mg-PSZ and Ce-PSZ overlap, implying that the particle sizes for both materials were approximately identical. In addition, a wide bimodal distribution presenting two maximum points, which are centered at around 0.1 μm was revealed. Conversely, in the Ca-PSZ sample, the results show a narrow distribution with fractions ranging from 3 μm to 20 μm.

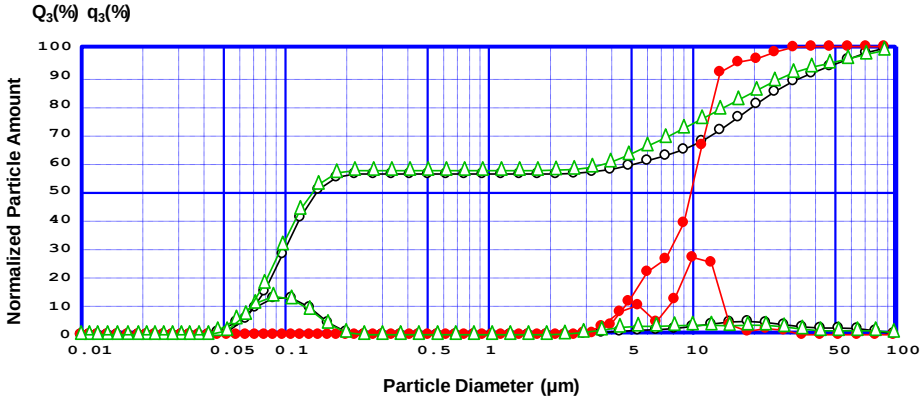

Figure 1. Differential and cumulative PSD curves of Mg-PSZ (black), Ca-PSZ (red) and Ce-PSZ (green) ceramics.

The results summarized in **Table 1** show that the Mg-PSZ and Ce-PSZ contain finer particles, with a mean value of 0.978 μm, and 0.851 μm, respectively, whereas larger particles were found for the Ca-PSZ, with a mean value of 9.030 μm. The modal and median diameters, defined for the cumulative distribution, are also shown.

Table 1. The results of particle size analyses of Mg-PSZ, Ca-PSZ and Ce-PSZ ceramics

Sample ID	Median D (μm)	Modal D (μm)	Mean V (μm)	SD*	D_{25} (μm)	D_{50} (μm)	D_{75} (μm)
Mg-PSZ	0.145	0.087	0.978	1.161	0.092	0.145	16.227
Ca-PSZ	9.808	9.993	9.030	0.192	6.858	9.808	11.930
Ce-PSZ	0.138	0.087	0.851	1.121	0.088	0.138	11.040

* SD- standard deviation

To determine the structural properties, XRPD analyses were performed on Ca-PSZ, Mg-PSZ, and Ce-PSZ samples with the XRPD patterns shown in **Figure 2.**

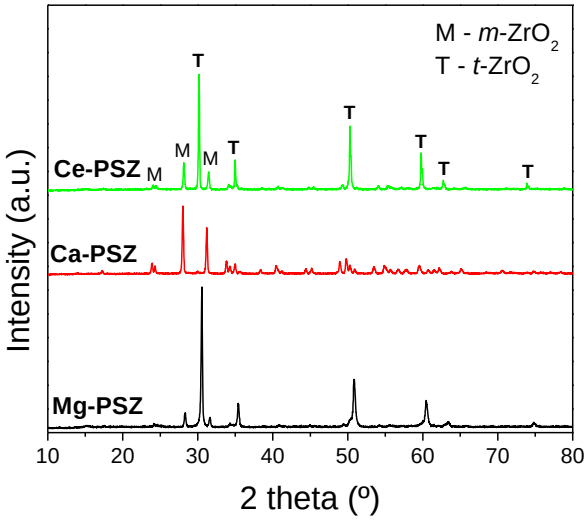

Figure 2. XRPD patterns of the prepared PSZ bulk ceramics.

Their examination revealed polymorphic powders because monoclinic (*m*-ZrO_2) and tetragonal (*t*-ZrO_2) structures are exhibited. For the phase identification the crystallographic information files corresponding to the pure monoclinic and tetragonal zirconia (*m*-ZrO_2, PDF # 96-152-8985; *t*-ZrO_2, PDF # 96-230-0613) phases from Crystallography Open Database (COD) of Match! Software were used.

The crystallite sizes of the prepared compositions were estimated using Scherrer equation:

$$D_{hkl}=0.9\lambda/(\beta\cos\theta) \quad (1)$$

where: D - crystallite size along (hkl) direction, β - full width half maximum (FWHM) of the most intense diffraction line, λ - wavelength of X-ray, θ - the Bragg angle [14].

The calculated *m*-ZrO_2 and *t*-ZrO_2 weight fractions, estimated using Match! software, and evolution of the crystallite sizes, determined by the Scherrer formula, are presented in **Table 2**. The calculated crystallite size of PSZ ranges in the nanometric domain, with the lowest value obtained for Ca-PSZ. The Mg-PSZ and Ce-PSZ powders are mainly composed of *t*-ZrO_2, with small peaks belonging to the *m*-ZrO_2 phase which are more evident in Ce-PSZ, whereas in the Ca-PSZ sample the predominant phase is *m*-ZrO_2. For the Mg-PSZ sample, the small difference between ionic radii of the Zr^{4+} (0.84 Å) and Mg^{2+} (0.72 Å), the substitution of Zr^{4+} on its lattice site by the Mg^{2+} ion is expected [2]. Furthermore, since Mg has the oxidation state of +2, it induces some oxygen vacancy in the structure which could be the main reason for the stabilization of the *t*-ZrO_2 phase [15]. In the case of Ca-PSZ, the increase in the lattice parameter is expected as the Ca^{2+} (1.00 Å) has a larger ionic radius than that of Zr^{4+}(0.86 Å). Substituting Ce with a higher ionic radius (0.97 Å) at Zr sites induces slight change in the lattice parameters. The mixture of *m*-ZrO_2 and *t*-ZrO_2 phases indicated that they were partially stabilized by the MgO, CaO, and CeO_2.

Table 2. The *t*- and *m*-ZrO_2 phase fractions and crystallite size calculated by Scherrer formula for the prepared PSZ materials.

Sample ID	***t*-ZrO_2 (wt.%)**	***m*-ZrO_2 (wt.%)**	**$D_{Scherrer}$* (nm)**
Mg-PSZ	79.2	20.8	47.79
Ca-PSZ	3.5	96.5	46.93
Ce-PSZ	66.6	33.4	59.98

The FTIR spectra of the prepared samples are displayed in Figure 3. Upon analyzing the spectra in the high-frequency region, it is evident that a broadband positioned around 3448 cm^{-1} is present in all three samples. This band is caused by the stretching vibration of the -OH group from the adsorbed water and is also visible in the low region as a sharp band of low intensity located at 1637 cm^{-1}.

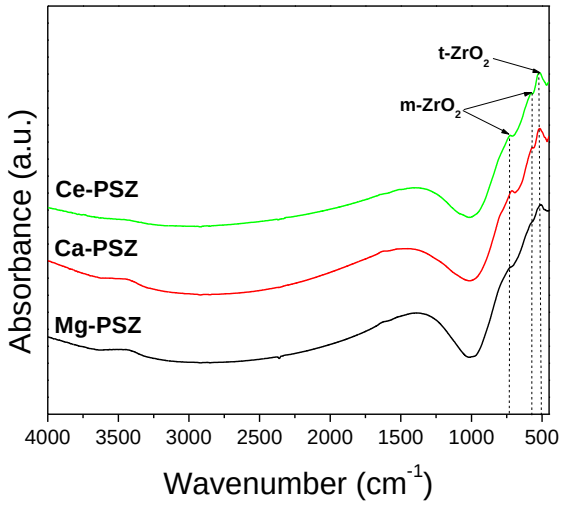

Figure 3. FTIR spectra of the prepared PSZ bulk ceramics.

Between 1600-1000 cm^{-1}, the broadband observed at ~ 1400 cm^{-1}, is likely due to the stretching mode vibration of Mg-O, Ca-O, or Ce-O bonds. [16]. The characteristic bands ascribed to the *m*-ZrO_2 are observed at 585 cm^{-1} and 735 cm^{-1}, and *t*-ZrO_2 is 529 cm^{-1} [17]. These results agree with the XRPD results where different phase ratio of *t*- and *m*-ZrO_2 phases were revealed, depending on the doping cations.

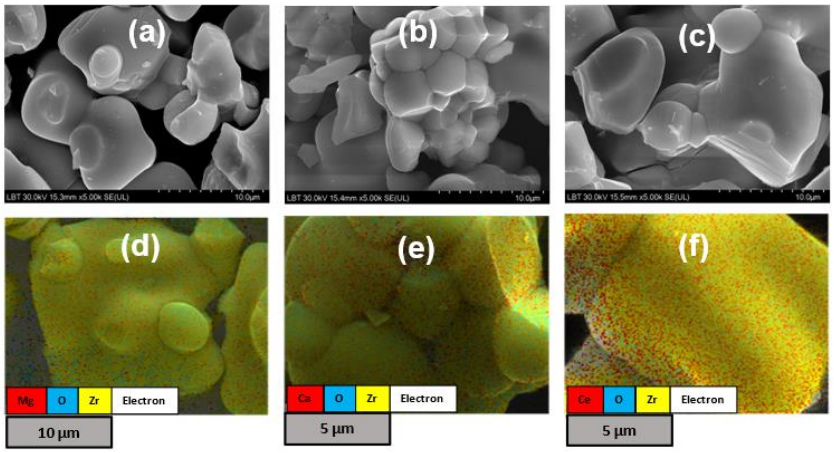

Figure 4. SEM images and corresponding elemental mapping of Mg-PSZ (a, d), Ca-PSZ (b, e), and Ce-PSZ (c, f), respectively

The results of morphological characterization of the prepared PSZ carried out using SEM are presented in **Figure 4a-c**. As shown irregular and agglomerated shapes like morphology were formed in the ceramic sample with grains interconnected to each other, as previously observed [18]. Qualitative analysis evaluated by elemental mapping (**Figure 4d-f**) confirmed the homogenous distribution of the elements in the PSZ samples. The results of elemental EDX analyses, displayed in **Figure 5** (right), accompanied by the SEM images of the surface of samples (left), confirmed the presence of the magnesium, calcium, cerium, zirconium, and oxygen elements. No other signals were detected, indicating the purity of the materials.

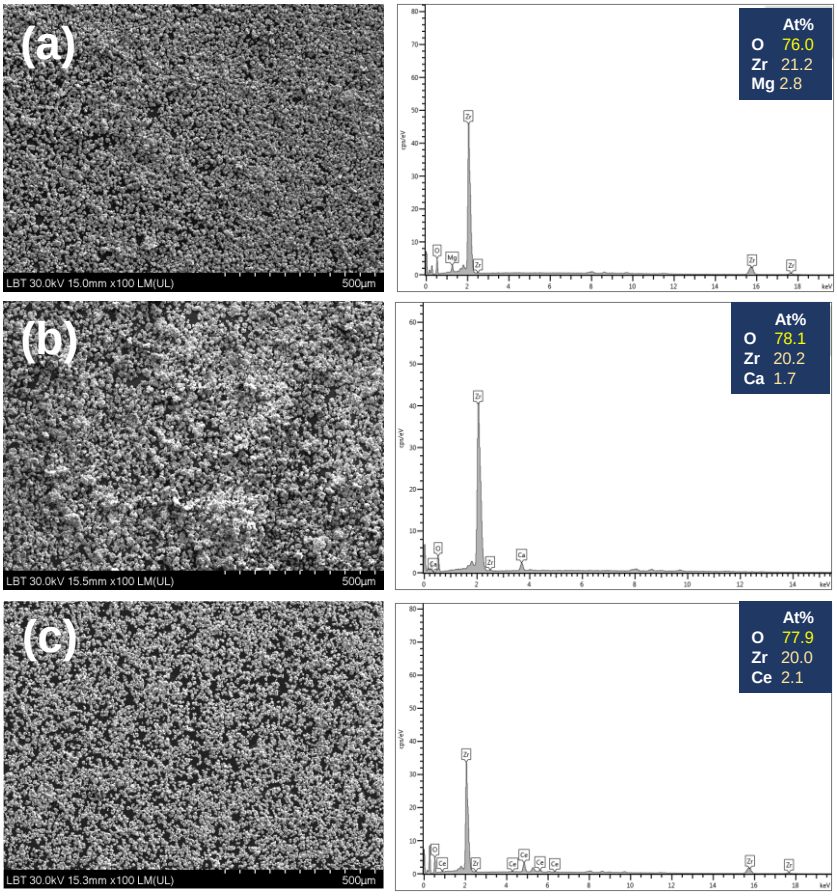

Figure 5. SEM images (left) under 100 X magnification and EDS (right) analysis for (a) Mg-PSZ, (b) Ca-PSZ and (c) Ce-PSZ.

The optical properties of the prepared compositions were considered in terms of UV-VIS DRS and the corresponding bandgaps (E_g) were calculated by Tauc plot using Kubelka-Munk function [19], as shown in **Figure 6a-d.** Depending on the types and chemical states of metal ions, the bandgaps of metal doped ZrO_2 varied, the differences being mainly associated with the electronic configurations of the ions, which control the energy levels in the ZrO_2. In our work, the determined bandgaps are 4.68 eV, 3.52 eV and 4.96 eV, for Mg-PSZ, Ca-PSZ, and Ce-PSZ, respectively. As know, ZrO_2 has a wide bandgap with the reported value of ~ 5.0 eV [20, 21]. The effects of Mg and Ca doping on the tetragonalization of the crystal structure and introduction of dopant states at the edge of the valence states below the Fermi level, as well as shifting the Fermi level towards the valence band maximum upon doping, have been previously demonstrated.

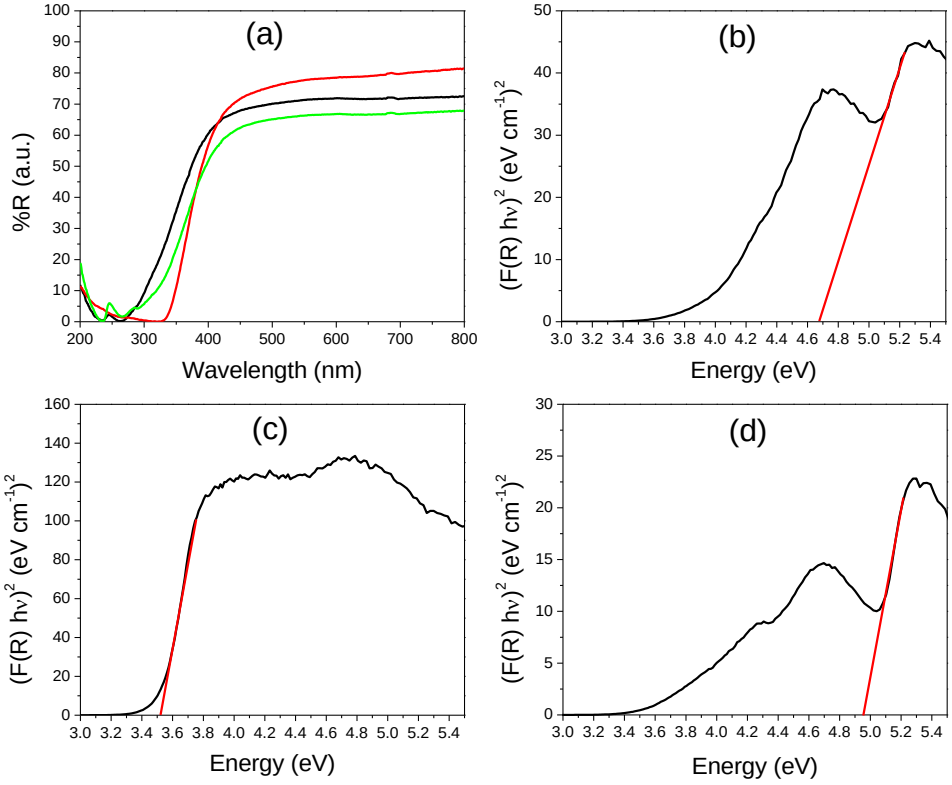

Figure 6. (a) UV-VIS DRS spectra of Mg-PSZ (black), Ca-PSZ (red) and Ce-PSZ (green) and corresponding Tauc plot for bandgap determination of (b) Mg-PSZ, (c) Ca-PSZ and (d) Ce-PSZ.

The reduced value of bandgaps on the doped zirconia may be due to the incorporation of the MgO, CaO or CeO_2. Recently, the role of oxygen vacancy in the RT stabilized *t*-ZrO_2 was investigated [22-25]. The presence of cerium stabilizes the metastable tetragonal phase at the expense of the monoclinic one [26]. Accordingly, the occupation of a regular crystal site by Ce^{4+} induces the formation of discrete defect levels inside the material bandgap constituted by the empty localized 4f orbitals of the lanthanide ion, thus drastically improving the visible light absorption by a two-step photon absorption mechanism [26]. It should also be noted that the stabilization mechanisms of the dopants are different: MgO and CaO stabilize the *t*-ZrO_2 phase by introducing anionic oxygen vacancies similar to Y_2O_3, whereas CeO_2 stabilizes the *t*-ZrO_2 phase by dilating the cation network decreasing the strain energy and the relief of oxygen overcrowding [27,28].

CONCLUSIONS

Bulk PSZ ceramic materials were successfully obtained by solid-state reaction at high temperature, followed by their characterization using laser diffraction, XRPD, FTIR, SEM/EDS and UV-VIS techniques. The structural analyses indicated the presence of both *m*- and *t*-ZrO_2 phases in different ratios, depending on the doping cation. Except for the Ca cation, which favoured the *m*-ZrO_2 phase formation, Mg and Ce played an important role in the tetragonalization of zirconia. Analysis by laser diffraction showed larger particle sizes compared to the calculated crystallite size, more pronounced in the Ca-PSZ, thereby confirming that this technique measures agglomerates and not individual particles. The SEM/EDS analysis confirmed the homogenous distribution of the elements through mixed oxide. Further, optical properties evaluated in terms of UV-VIS DRS spectra, revealed that the doped ZrO_2 samples showed a smaller bandgap compared with pure ZrO_2, which may be due to the incorporation of magnesia, calcia or ceria in the ZrO_2 matrix. Doping ZrO_2 represents an interesting approach to manipulating its bandgap, making these materials attractive in various applications, ranging from optoelectronics to prosthodontics, with the biomedical and bioengineering domains being of great importance.

EXPERIMENTAL SECTION

The PSZ ceramic materials were prepared by solid state reaction at high temperature. To obtain 10 at% Mg, Ca or Ce in ZrO_2, starting powders of ZrO_2 (Riedel-de Haën AG, Germany, 99%), CaO (Alfa Aesar, Germany, 99.95%), MgO (Alfa Aesar, Germany, 99.99%) and CeO_2 (LOBA Feinchemie GmbH, Austria,

99.95%) were used as raw materials. The mixture of different oxides was grounded using an agate mortar and pestle, and then heated in an alumina crucible in air using an Nabertherm LHT 04/16 high-temperature furnace (Lilienthal, Germany), first at 900 °C and then at increasing temperatures from 1000 °C up to 1600 °C. At each time, the 12h annealings were followed by air quenching and regrinding of the mixtures.

Synthesized Mg-PSZ, Ca-PSZ and Ce-PSZ ceramics were further characterized using different methods.

The PSD of the prepared powdered ceramics was measured in suspension using a micro- and nanoparticle analyzer SALD-7101 (Shimadzu, Japan). For the measurements, the samples were immersed for 15 s in distilled water used as a solvent, with aggregation being reduced using treatment with ultrasounds.

XRPD analysis was performed to investigate the structure of the samples using a Shimadzu XRD-6000 diffractometer operating at 40 kV, 30 mA, with Ni-filter and graphite monochromator for CuKα (λ=1.54060 Å). The diffraction patterns were recorded in the 2θ range of 10–80° at a scan speed of 2 °/min.

FTIR measurements were performed using a Jasco FTIR 6200 spectrometer. The spectra were recorded from KBr pellets, with a spectral resolution of 4 cm^{-1}.

For the morphological analyses, the SEM/EDS images were obtained at 30 kV with different magnifications using a Hitachi SU8230 (Tokyo, Japan) microscope. The electron microscope was coupled with an Aztec X-Max 1160 EDX detector (Oxford Instruments).

UV-VIS spectroscopy was employed to characterize the influence of the dopants on the optical properties of the ZrO_2 ceramics. DRS spectra were registered with a double-beam JASCO V-650 (Japan) spectrophotometer, equipped with an ISV-722 Integrating Sphere, in the wavelength range from 200 to 800 nm, with a scan rate of 400 nm/min.

ACKNOWLEDGMENTS

Authors gratefully acknowledge Assoc. Prof. Lucian Barbu-Tudoran for SEM/EDS measurements.

REFERENCES

1. A.K. Chitoria; A. Mir; M.A. Shah; *Ceram. Int.,* **2023,** 49, 32343-32358.
2. L. Bizo, M; Mureşan-Pop; R. Barabás; L. Barbu-Tudoran; A. Berar; *Materials,* **2023**, *16*, 2680.

3. D. Yusuf; E. Maryani; D.F. Mardhian; A.R. Noviyanti; Molecules, **2023,** *28*, 6054.
4. K. Wahyudi; E. Maryani; F. Arifiadi; A. Rostika; D. Yusuf; R.J. Manullang, Suyanti; R. Septawendar; *Mater. Res. Express,* **2021,** *8*, 045022.
5. J. Cho; B. Yang; C. Shen; H. Wang; X. Zhang; *J. Eur. Ceram.*, **2023**, *43*, 3, 1098-1107.
6. J. Wang; D. Chu; H. Ma; S. Fang; Q. Chen; B. Liu; G. Ji; Z. Zhang; X. Jia; *Ceram. Int.*, **2021**, *47*, 15180-15185.
7. L. Zhao; S. Yao; L. Kang; H.Y. Sun; Q. Huang; *Sci. Adv. Mater.*, **2019**, *11*, 4, 483-488.
8. L. Hwanseok; J. Kanghee; L. Heesoo; *J. Surf. Sci. Eng*. **2021**, *6*, 38.
9. M.V. Peirani; E. Brandaleze; *Sch. J. Eng. Technol.* **2017**, *5,* 280-289.
10. Y.T. Sung; J.H. Son; S.S. Lee; D.S. Bae; *Korean J. Mater. Res.,* **2014**, *24*, 53-59.
11. A.A. Ali; S.A. Shama; A.S. Amin; S.R. EL-Sayed; *Mat. Sci. Eng. B*, **2021,** 269, 115167.
12. J. K. Mbae; Z.W. Muthui; *Helyon*, **2023,** *9*, e20998.
13. S.R. Gul; M. Khan; Y. Zeng; M. Lin; B. Wu; C.-T. Tsai; *Materials,* **2018**, *19*, 1238.
14. A.L. Patterson; *Phys. Rev.*, **1939**, *56*, 978-982.
15. M.S. Khan; M.S. Islam; D.R. Bates; *J. Mater. Chem.,* **1998,** *8*, 2299-2307.
16. G. Balakrishnan; R. Velavan; K.M. Batoo; E.H. Raslan; *Results Phys.*, **2020,** *16*, 103013.
17. S. Sagadevan; J. Podder; I. Das; *J. Mater. Sci.: Mater. Electron.* **2016,** 27, 5622–5627.
18. A. Berar; M. Mureșan-Pop; L. Barbu-Tudoran; R. Barabás; L. Bizo; *Studia UBB Chemia*, **2020**, *LXV, 2,* 221-232.
19. P. Kubelka; F. Munk-Aussig; *Physik*, **1931**, *12*, 593-601.
20. L. Xie; J. Wang; Y. Hu; S. Zhu; Z. Zheng; S. Weng; P. Liu; *RSC Adv.,* **2012,** *2*, 9881-9886.
21. H.M. Shinde; T.T. Bhosale; N.L. Gavade; S.B. Babar; K.M. Garadkar; *J. Mater. Sc.i: Mater. Electron.,* **2018,** *29*, 14055-14064.
22. D. Sangalli; A. Lamperti; E. Cianci; R. Ciprian; M. Perego; A. Debernardi; *Phys. Rev. B*, **2013,** *87*, 085206.
23. N. Shuai; Z. Peng; X. Qian; L. Zhengcao; Z. Zhengjun; *J. Phys. D: Appl. Phys*., **2013,** *46*, 445004.
24. Y. Xie; Z. Ma; L. Liu; Y. Su; H. Zhao; Y. Liu; Z. Zhang; H. Duan; J. Li; E. Xie; *Appl. Phys. Lett.,* **2010,** *97*, 141916.
25. G. Lucovsky; C.L. Hinkle; C.C. Fulton; N.A. Stoute; H. Seo; J. Lüning; *Radiat. Phys. Chem.* **2006,** *75*, 2097-2101.
26. E. Gaggero; P. Calza; E. Cerrato; M.C. Paganini; *Catalysts*, **2021**, *11*, 1520.
27. P. Li; I.-W. Chen; J.E. Penner-Hahn; *J. Am. Ceram. Soc.* **1994,** *77*, 1281-1288.
28. S.Y. Kwon; I.H. Jung; *J. Eur. Ceram. Soc.*, **2017,** *37*, 1105-1116.